JOURNAL OF GEOPHYSICAL RESEARCH: PLANETS, VOL. 118, 952–962, doi:10.1002/jgre.20087, 2013

Global dust storm signal in the meteorological excitation of Mars' rotation

Y. H. Zhou,[1] D. A. Salstein,[2] X. Q. Xu,[1] and X. H. Liao[1]

Received 24 July 2012; revised 7 March 2013; accepted 25 April 2013; published 16 May 2013.

[1] The meteorological excitation of Mars' rotation refers to the change of Mars' orientation parameters caused by meteorological processes, e.g., that portion due to variations of atmospheric circulation and surface pressure, and a cryospheric part due to the variable Martian polar ice caps associated with the CO_2 sublimation/condensation effects. Global dust storms (GDSs) are unique meteorological events on Mars that cause changes in surface pressure, polar caps extent, and circulation patterns on a global scale, which in turn alter Mars' rotation under the conservation of Mars' total angular momentum. In this paper, the GDS signal in the meteorological excitation of Mars' rotation is investigated on seasonal, diurnal, and semidiurnal time scales, based on the Martian Climate Database. On seasonal scales, the cryospheric excitation plays a less important role in general, due to its location at high latitudes, than its atmospheric counterpart. The GDS brings (−3%, +15%) changes in the amplitude of annual polar motion and length-of-day (LOD) variation and (+22%, −34%) changes in the amplitude of semiannual polar motion and LOD variation. On diurnal and semidiurnal scales, the cryospheric excitation can be fully neglected in comparison to its atmospheric counterpart. A significant GDS signal is found with respect to the diurnal polar motion and semidiurnal LOD excitation variation, because of strong atmospheric tides arising from GDS effects. The amplitude increases in diurnal polar motion and semidiurnal LOD variation during some periods of the Martian year may reach 3–5 times as large as those during the same stage in a typical Martian year.

Citation: Zhou, Y. H., D. A. Salstein, X. Q. Xu, and X. H. Liao (2013), Global dust storm signal in the meteorological excitation of Mars' rotation, *J. Geophys. Res. Planets*, *118*, 952–962, doi:10.1002/jgre.20087.

1. Introduction

[2] The meteorological excitation of Mars' rotation refers to the change of Mars' orientation parameters (length-of-day (LOD) variation and polar motion) caused by meteorological processes, e.g., an atmospheric part due to variations of atmospheric circulation and surface pressure and a cryospheric part due to the variable Martian polar ice caps associated with the CO_2 sublimation/condensation effects. This subject has been under extensive investigations [*Philip*, 1979; *Cazenave and Balmino*, 1981; *Chao and Rubincam*, 1990; *Yoder and Standish*, 1997; *Defraigne et al*., 2000; *Van den Acker et al*., 2002; *Sanchez et al*., 2003, 2004; *Karatekin et al*., 2006a, 2011a, 2011b; *Konopliv et al*., 2011], based on Mars general circulation models (GCMs) [*Forget et al*., 1999; *Haberle et al*., 1999] and space observations [*Folkner et al*., 1997; *Smith et al*., 2001; *Litvak et al*., 2004; *Karatekin et al*., 2006b; *Konopliv et al*., 2006, 2011].

[3] Global dust storms (GDSs), known also as planet-encircling storms, are unique meteorological events that occur irregularly on Mars about every three Martian "years" [*Zurek and Martin*, 1993; *Gawrych*, 2007]. During the period of these events, a great amount of suspended dust lifted by the winds modifies the radiative properties of the atmosphere. It causes changes in surface temperature and pressure, polar cap extent, and circulation patterns on a global scale [*Cantor*, 2007; *Smith*, 2008; *Elteto and Owen*, 2010], which in turn alter Mars' rotation under the conservation of Mars' total angular momentum. However, while a number of investigations have concerned the meteorological excitation of Mars' rotation, few studies have involved the GDS effect, and none have examined the results on the short diurnal and semidiurnal time scales.

[4] *Van den Acker et al*. [2002] first examined the GDS influence on the meteorological excitation of Mars' rotation on seasonal time scales. They showed that a variation of the effect can be expected in Mars' annual/semiannual rotational rate. Note, however, that they considered this result to be preliminary, owing to available data during only three Martian "months," a span that has now been significantly extended.

[1]Shanghai Astronomical Observatory, Chinese Academy of Sciences, Shanghai, China.
[2]Atmospheric and Environmental Research, Lexington, Massachusetts, USA.

Corresponding author: Y. H. Zhou, Shanghai Astronomical Observatory, Chinese Academy of Sciences, Shanghai 200030, China. (yhzhou@shao.ac.cn)

2169-9097/13/10.1002/jgre.20087

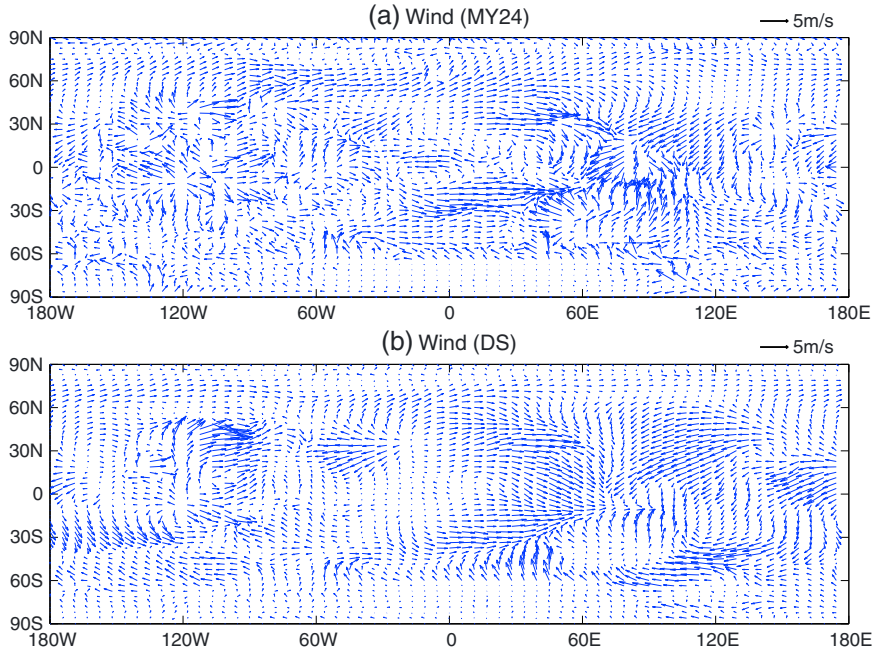

Figure 1. (a, b) The mean horizontal wind over 200 m altitude at hour 12 of a Martian day in "month" 8 (unit in m/s) for the "Martian Year 24 (MY24)"/"dust storm (DS)" scenarios. The MY24 scenario was designed to mimic Mars during a typical Martian year based on the observations of the Mars Global Surveyor. The DS scenario represented Mars during a global dust storm, which is only available when such storms are likely to happen during southern spring and summer.

[5] Noting the important role of dust on atmospheric dynamics and planetary rotation, *Konopliv et al.* [2011] suggested though that different assumptions for the atmospheric dust content change the LOD solution of the Martian Climate Database (MCD) by about +15% for $0 < Ls < 250°$ and up to +30–50% for $Ls > 250°$, where Ls is the solar longitude of Mars. *Karatekin et al.* [2011a] showed that the effects of different atmospheric dust scenarios on Mars' LOD change. The largest variations in LOD variation occur during the southern summer, when the planet is near perihelion.

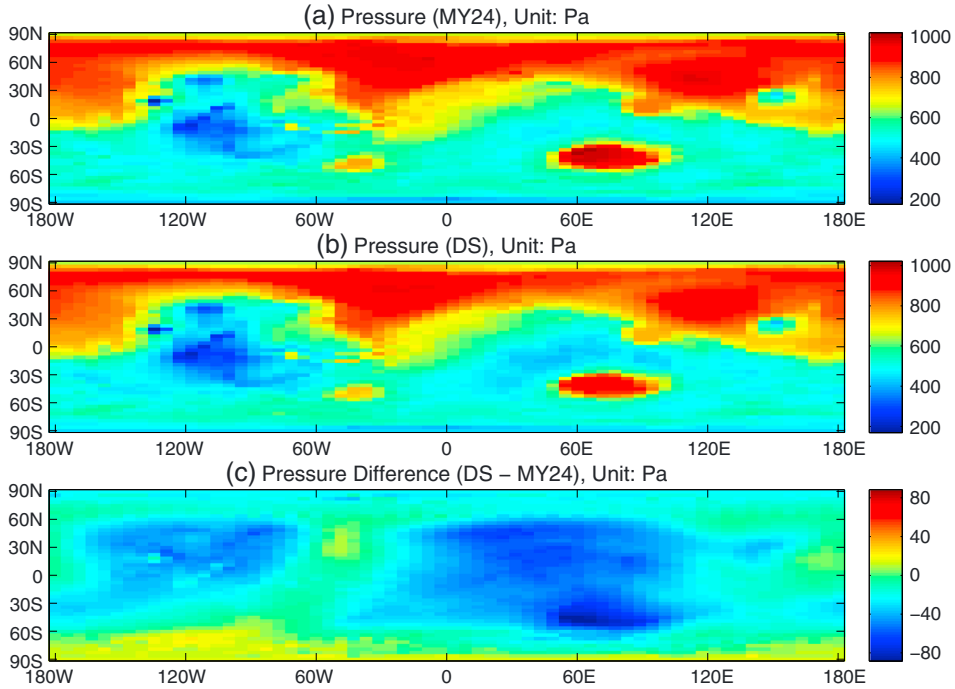

Figure 2. (a, b) Surface pressure at hour 12 of a Martian day in month 8 (unit in Pa) for the MY24/DS scenarios and (c) the pressure difference between the DS and MY24 scenarios.

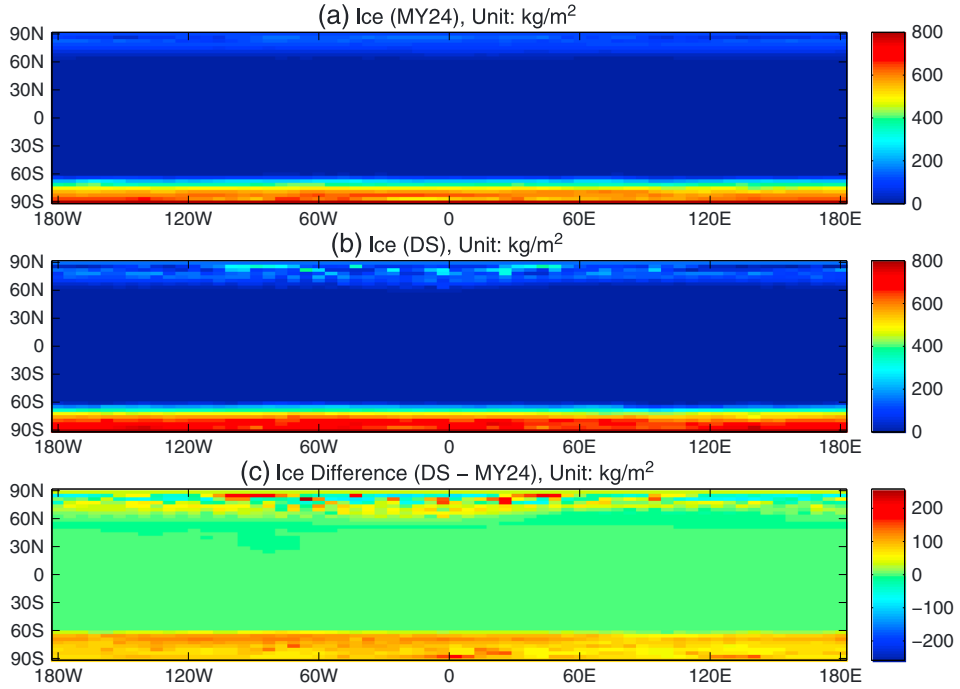

Figure 3. (a, b) The surface density of ice at hour 12 of a Martian day in month 8 (unit in kg/m^2) for the MY24/DS scenarios and (c) the ice difference between the DS and MY24 scenarios.

[6] GDSs can affect signals of meteorological excitations of Mars' rotation on very short time scales (e.g., diurnal/semidiurnal time scales) [*Bridger and Murphy*, 1998]. The physical mechanisms at work on the diurnal/semidiurnal time scales relate primarily to atmospheric tides. While the redistribution of CO_2 mass between the Martian atmosphere and the polar caps plays an important role in exciting seasonal variations of Mars' rotation, it is expected to contribute little to the Mars' diurnal/semidiurnal rotational change. The studies on short-period time scales may provide a new viewpoint to assess GDS impacts and further our understandings of Mars' rotational dynamics, which in turn can yield important information about the planet's internal structure as well as serve for eventual navigation uses.

[7] The objective of this paper is twofold: (1) to study comprehensively the seasonal GDS signals in the meteorological excitation of Mars' rotation, using the enhanced MCD (version 4.3) data which have been recently made available [*Millour et al.*, 2011] (see section 2.1 for a detailed description of MCD v4.3); and (2) to go beyond previous studies by examining the diurnal and semidiurnal effects, which also relate to the tides. The structure of the paper is as follows. In section 2, we introduce the MCD data and meteorological impacts of GDSs. Section 3 presents the theoretical formulation for computing Mars' rotational excitation functions. Studies of the GDS signal in the meteorological excitation of Mars' rotation are given in section 4. We summarize and discuss the results in section 5.

2. MCD Data and Meteorological Impacts of GDS

2.1. MCD Data

[8] The MCD is a database of statistics describing the climate and environment of the Martian atmosphere [*Forget et al.*, 1999]. It is constructed on the basis of outputs from a general circulation model (GCM) developed by the Laboratoire de Météorologie Dynamique du CNRS, France, in collaboration with the University of Oxford, UK, and the Instituto de Astrofisica de Andalucia, Spain. The MCD is constructed from a GCM of Martian atmospheric dynamics based on physical principles and extensively validated by observations [*Forget et al.*, 1999; *Hourdin et al.*, 1993, 1995; *Lewis et al.*, 1999]. The GCM uses many physical parameterizations, such as built-in topography and thermal inertia models, to describe the atmospheric circulation over the Martian topography. It

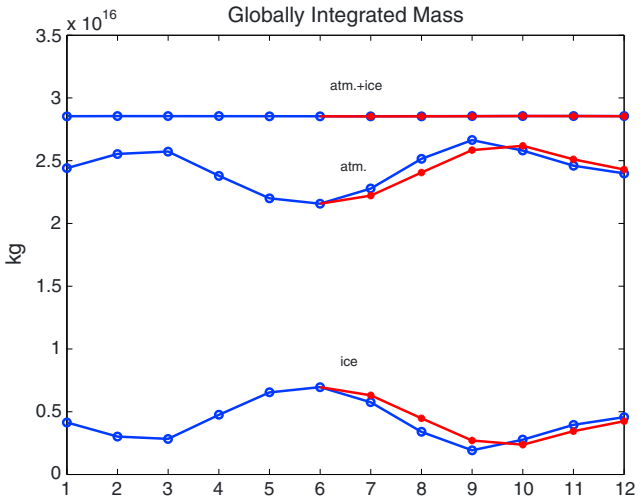

Figure 4. The globally integrated mass of atmosphere, ice, and their sum during months 1–12 in a Martian year for the MY24/DS scenarios (blue/red curves and open/closed circles).

Table 1. Parameters of Mars and Their Values With References

Parameter	Value	Units	Reference
Ω	0.7088 (10^{-4})	s^{-1}	*Smith et al.* [1999]
T_c	200	days	*Defraigne et al.* [2000]
Λ_0	88775	s	*Sanchez et al.* [2003]
R	3396000	m	*Smith et al.* [1999]
C	2.69956 (10^{36})	$kg\,m^2$	*Sanchez et al.* [2004]
A	2.68594 (10^{36})	$kg\,m^2$	*Sanchez et al.* [2004]
g	3.71	$m\,s^{-2}$	*Smith et al.* [1999]
k_2	0.153		*Yoder et al.* [2003]
k'_2	−0.06		*Sanchez et al.* [2004]
k	1.2015		*Lambeck* [1980]
k_r	0.9987		*Barnes et al.* [1983]

is believed to represent the current best knowledge of the state of the Martian atmosphere.

[9] Two scenarios of the MCD are employed to investigate the GDS signal in the meteorological excitation of Mars' rotation. One scenario, named "Martian Year 24 (MY24)" (24th Martian year according to the calendar proposed by *Clancy et al.* [2000]), was designed to mimic Mars during a typical Martian year, based on the observations of the Mars Global Surveyor (MGS) from January 1999 to June 2001. The dust fields were derived from MGS thermal emission spectrometer observations using a data assimilation technique. The MY24 scenario represented the average climate on Mars, i.e., a moderately dusty Mars without GDSs.

[10] The MY24 scenario contains simulated data (e.g., CO_2 ice cover, atmospheric surface pressure, atmospheric density, zonal (eastward) wind, meridional (northward) wind) stored on a 5.625° by 3.75° longitude-latitude grid from the surface up to an approximate altitude of 270 km. Fields are averaged and stored 12 times a Martian day at Martian "hours" 2, 4, 6, 8, 10, 12, 14, 16, 18, 20, 22, and 24 for each of 12 Martian "months" per Martian year. Each month covers 30° in solar longitude and is approximately two Earth months long.

[11] Another scenario, named "dust storm (DS)," represented Mars during a GDS (dust opacity set to $\tau = 4$). The data format of DS is similar to that of MY24, except that it is only available when such storms are likely to happen during southern spring and summer (solar longitude Ls = 180°–360°), when the solar insolation reaches a maximum.

[12] The latest MCD v4.3 includes a more realistic representation of the CO_2 cycle and an improved radiative transfer procedure using updated radiative properties of dust [*Millour et al.*, 2011]. It covers six Martian months of a typical GDS, 3 months longer than the MCD v3.0 used by *Van den Acker et al.* [2002]; this extension in time period will allow an in-depth investigation of the GDS effect.

2.2. Meteorological Impacts of GDS

[13] The meteorological impacts of GDSs are examined by comparing the wind pattern, the surface pressure, and the surface density of ice, between the MY24 and DS scenarios.

[14] Figure 1 shows the mean horizontal wind over 200 m altitude at hour 12 of a Martian day in "month" 8 (unit in m/s), for the MY24/DS scenarios. Obviously, the wind patterns change significantly with the presence of the GDS. The DS winds appear to have in general less high resolution than do the MY24 winds.

[15] Figure 2 exhibits the global distribution of surface pressure at hour 12 of a Martian day in month 8 (unit in Pa) for the MY24/DS scenarios as well as the pressure difference between them. Unlike the horizontal wind, the general pattern of surface pressure, e.g., the dichotomy in air pressure between the northern and southern hemispheres relative to Mars' remarkable topography [*Wieczorek*, 2007], remains unchanged. And air pressures decrease in the DS scenario generally in most areas by at most approximately 5% in magnitude.

[16] The surface density of ice at hour 12 of a Martian day in month 8 (unit in kg/m^2) for the MY24/DS scenarios and their differences in ice signal are displayed in Figure 3. Most of the ice appears in south polar areas, and the ice increases generally due to the GDS by up to about 30% in some places. The increase of ice is in line with decreasing air pressure shown in Figure 2, as expected from the mass balance within the Mars' atmosphere and cryosphere.

[17] Further details of mass balance on Mars are shown in Figure 4, namely, globally integrated mass of atmosphere, ice, and their sum during months 1–12 in a Martian year, for the MY24/DS scenarios (blue/red curves and open/closed circles). Here the GDS acts to decrease the atmospheric mass and simultaneously increase the mass of ice before month 10 and vice versa after month 10. The total mass of atmosphere and ice maintains the global mass balance. This global result follows the regional results shown in Figures 2 and 3.

3. Mars' Rotation Excitation Function

[18] In the Martian coordinate system, the rotation of Mars can be described by the three-dimensional instantaneous angular velocity vector of the mantle. Its axial and equatorial

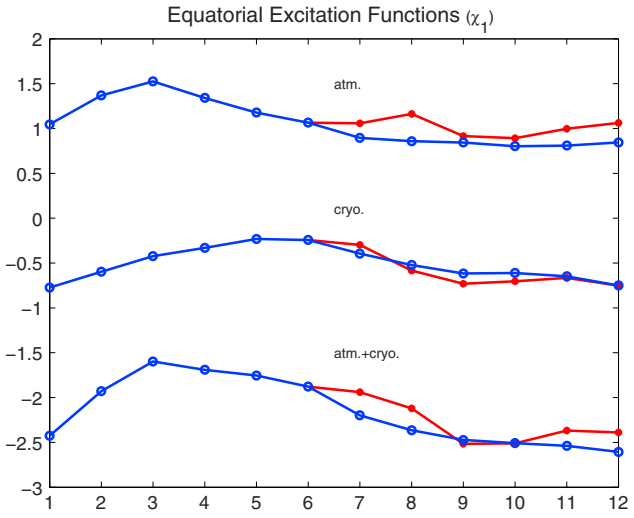

Figure 5. The equatorial excitation functions (χ_1) during months 1–12 in a Martian year for the MY24/DS scenarios (blue/red curves and open/closed circles). Unit is 10^{-7}. The curves are vertically shifted for clarity of display. atm.: atmospheric excitation function; cryo.: cryospheric excitation function.

Table 2. Amplitude and Phase of the Seasonal Polar Motion for the "Martian Year 24 (MY24)"/"Dust Storm (DS)" Scenarios[a]

	MY24 Scenario		DS Scenario	
	Amplitude (mas)	Phase (deg)	Amplitude (mas)	Phase (deg)
Annual polar motion: x component				
Atm. Contrib.	9.2	2.2	6.3	2.1
Cryo. Contrib.	6.9	−59.1	7.8	−53.1
Total Contrib.	13.9	−23.7	12.5	−28.7
Annual polar motion: y component				
Atm. Contrib.	14.8	4.3	18.3	−0.7
Cryo. Contrib.	1.9	11.0	9.3	120.1
Total Contrib.	16.7	5.1	15.7	29.9
Semiannual polar motion: x component				
Atm. Contrib.	5.6	−57.1	4.9	−40.3
Cryo. Contrib.	3.4	−157.3	3.3	164.5
Total Contrib.	6.0	−90.5	2.3	−76.2
Semiannual polar motion: y component				
Atm. Contrib.	5.5	79.6	7.7	66.2
Cryo. Contrib.	4.6	−72.1	12.2	−148.0
Total Contrib.	2.6	23.6	7.2	175.2

[a]The MY24 scenario was designed to mimic Mars during a typical Martian year based on the observations of the Mars Global Surveyor. The DS scenario represented Mars during a global dust storm, which is only available when such storms are likely to happen from "months" 7–12. The phase angle refers to the beginning of a Martian year with respect to the sine convention. Atm. Contrib.: Atmospheric Contribution; Cryo. Contrib.: Cryospheric Contribution; mas: milliseconds of arc.

components are associated with the variations of Mars' rotational rate (or the length-of-day (LOD) change) and the polar motion, respectively. As is the case for Earth, Mars' rotation is basically subject to the following excitation equations, under the conservation of Mars' total angular momentum [*Barnes et al.*, 1983; *Eubanks*, 1993; *Van den Acker et al.*, 2002; *Zhou et al.*, 2006]:

$$\mathbf{m} + (i/\sigma_c)\dot{\mathbf{m}} = \boldsymbol{\chi} - (i/\Omega)\dot{\boldsymbol{\chi}} \tag{1}$$

$$m_3 = -\chi_3. \tag{2}$$

[19] In equation (1), $\mathbf{m} = m_1 + im_2$ is a dimensionless complex-valued small quantity representing Mars' polar motion, where subscripts 1 and 2 refer to the x (along the 0° meridian) and y (along the 90° east meridian) coordinates of the Martian reference frame. Here $\boldsymbol{\chi} = \chi_1 + i\chi_2$, with χ_1 and χ_2 being the x and y components, respectively, of the polar motion excitation function; Ω is the mean angular velocity. $\sigma_c = 2\pi/T_c$ is the Chandler frequency, whose period T_c is Mars' free Eigen-period, related to the difference between the planet's polar and equatorial moment of inertia and elasticity [*Sanchez et al.*, 2004]. In this study, we adopt a value of 200 days for this Chandler period [*Defraigne et al.*, 2000; *Van Hoolst et al.*, 2000; *Van den Acker et al.*, 2002].

[20] In equation (2), $m_3 = -\Delta\Lambda/\Lambda_0$, the small fractional change in LOD, where Λ_0 and $\Delta\Lambda$ are a standard LOD and its deviation, subscript 3 refers to the z (along the north pole) coordinate of the Martian frame, and χ_3 is the excitation function for the LOD change.

[21] The Mars rotation excitation functions ($\boldsymbol{\chi}$ and χ_3) consist of an atmospheric part ($\boldsymbol{\chi}^{\mathrm{atm}}$ and χ_3^{atm}) due to variations of surface pressure and atmospheric winds and a cryospheric part ($\boldsymbol{\chi}^{\mathrm{cryo}}$ and χ_3^{cryo}) from changes in the mass of polar ice caps. When considering the core as solid and rigidly coupled with the mantle, these functions are expressed as follows [e.g., *Eubanks*, 1993]:

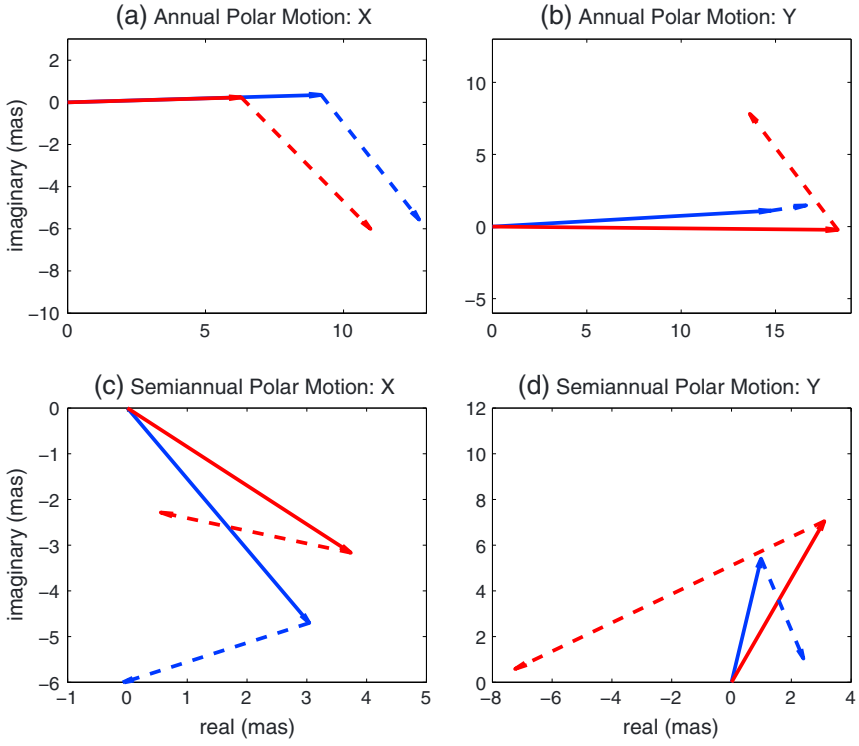

Figure 6. Phasor diagrams of the annual and semiannual polar motion due to the atmospheric/cryospheric excitations (solid/dashed phasors) for the MY24/DS scenarios (blue/red phasors).

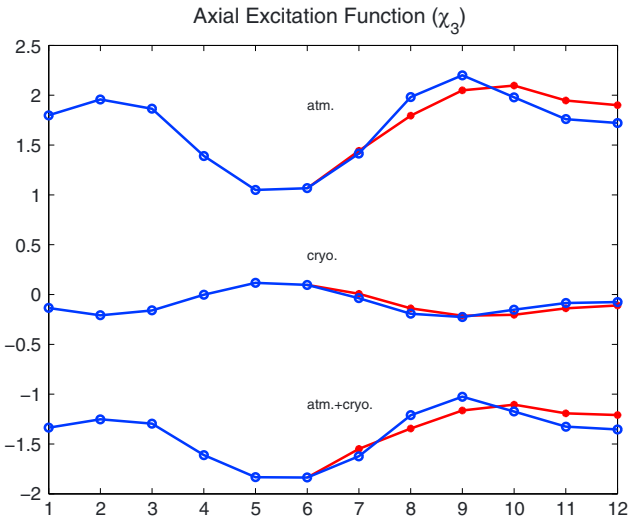

Figure 7. The axial excitation functions (χ_3) during months 1–12 in a Martian year for the MY24/DS scenarios (blue/red curves and open/closed circles). Unit is 10^{-8}. The curves are vertically shifted for clarity of display.

$$\boldsymbol{\chi}^{\mathrm{atm}} = \frac{-R^3 k}{g\Omega(C-A)(k-k_2)}\left[(1+k'_2)\Omega R\iint p_s \sin\varphi\cos^2\varphi e^{i\lambda}\mathrm{d}\lambda\mathrm{d}\varphi + \iiint (u\sin\varphi + iv)\cos\phi e^{i\lambda}\mathrm{d}p\mathrm{d}\lambda\mathrm{d}\varphi\right] \tag{3}$$

$$\chi_3^{\mathrm{atm}} = \frac{R^3 k_r}{g\Omega C}\left[\left(1+k'_2\right)\Omega R\iint p_s\cos^3\varphi\mathrm{d}\lambda\mathrm{d}\varphi + \iiint u\cos^2\varphi\mathrm{d}p\mathrm{d}\lambda\mathrm{d}\varphi\right] \tag{4}$$

$$\boldsymbol{\chi}^{\mathrm{cryo}} = \frac{-R^4 k\left(1+k'_2\right)}{(C-A)(k-k_2)}\iint q_{\mathrm{ice}}\sin\varphi\cos^2\varphi e^{i\lambda}\mathrm{d}\lambda\mathrm{d}\varphi \tag{5}$$

$$\chi_3^{\mathrm{cryo}} = \frac{R^4 k_r\left(1+k'_2\right)}{C}\iint q_{\mathrm{ice}}\cos^3\varphi\mathrm{d}\lambda\mathrm{d}\varphi, \tag{6}$$

[22] Where R is Mars' mean radius, C and A Mars' principal moments of inertia, g gravitational acceleration, k_2 the second-order volumetric number, k'_2 the second-order load Love number, k the secular Love number computed from $k = \frac{2(C-A)G}{\Omega^2 R^5}$ [*Lambeck*, 1980], k_r the rotational Love number computed from $k_r = \frac{1}{1+2k_2(C-A)/(kC)}$ [*Barnes et al.*, 1983], λ and φ longitude and latitude at a given grid point, p_s surface pressure, q_{ice} the surface mass density of the polar ice caps, and u and v the zonal and meridional wind velocities, respectively.

4. GDS Signal in the Meteorological Excitation of Mars' Rotation

[23] Here we employ a model of a solid Mars for simplicity [*Sanchez et al.*, 2004], as the differences between the effects for a liquid and a solid core are smaller than 1% of the total effect in Mars' polar motion and LOD variations [*Defraigne et al.*, 2000]. The atmospheric and cryospheric excitation functions are computed using the latest MCD v4.3 data on the basis of equations (3)–(6). Table 1 lists the values of parameters used in the calculations.

[24] In calculating the atmospheric excitation function due to the variability of atmospheric circulation, we integrate wind from Mars' topographic surface to the top of the model in a similar way as we computed the atmospheric excitation function on Earth [*Zhou et al.*, 2006]. The wind excitation comes predominately from the lower atmosphere (under 130 km), with that from the upper atmosphere (over 130 km) being 2 orders of magnitude smaller.

4.1. Seasonal Time Scales

4.1.1. Polar Motion

[25] The DS scenario contains data only for the latter half of a Martian year. We supplement the data of the early half year with that of the MY24 scenario. Following the approach of *Zhou et al.* [2006] but tailored for Mars instead of Earth, we examine the GDS signal in the meteorological excitation of Mars' rotation on seasonal time scales.

[26] Figure 5 displays the equatorial excitation functions (χ_1) during months 1–12 in a Martian year for the MY24/DS scenarios (blue/red curves and open/closed circles). The χ_2 component (not shown) exhibits a similar style as χ_1. The curves are vertically shifted for clarity of display. The GDS signal is visible. The cryospheric excitation plays in general a less important role than its atmospheric counterpart due to the low weighting in the excitation functions at its high-latitude location, though it is still non-negligible.

[27] Table 2 lists the least-squares fitted amplitude and phase of seasonal polar motion contributed from the atmosphere and cryosphere for the MY24/DS scenarios. The phase angle refers to the beginning of a Martian year with respect to the sine convention. The Phasor diagrams of the annual and semiannual polar motion due to the atmospheric/cryospheric excitations (solid/dashed phasors) for the MY24/DS scenarios (blue/red phasors) are displayed in Figure 6.

[28] For the GDS signal on annual polar motion, the atmospheric excitation decreases the amplitude of x component but increases that of the y component, while the cryospheric excitation effect is to increase the amplitudes of both x and y components. In total, the GDS decreases the amplitude of the annual polar motion by 3%.

[29] For the GDS signal on semiannual polar motion, the atmospheric and cryospheric excitations decrease the amplitude of the x component but increase that of the y

Table 3. Amplitude and Phase of the Seasonal LOD Variations for the MY24/DS Scenarios[a]

	MY24 Scenario		DS Scenario	
	Amplitude (ms)	Phase (deg)	Amplitude (ms)	Phase (deg)
Annual LOD variation				
Atm. Contrib.	0.318	133.6	0.374	126.5
Cryo. Contrib.	0.084	−50.6	0.107	−57.1
Total Contrib.	0.234	135.1	0.268	127.9
Semiannual LOD variation				
Atm. Contrib.	0.310	−36.3	0.224	−43.1
Cryo. Contrib.	0.108	152.5	0.089	141.0
Total Contrib.	0.204	−40.9	0.135	−45.8

[a]The phase angle refers to the beginning of a Martian year with respect to the sine convention.

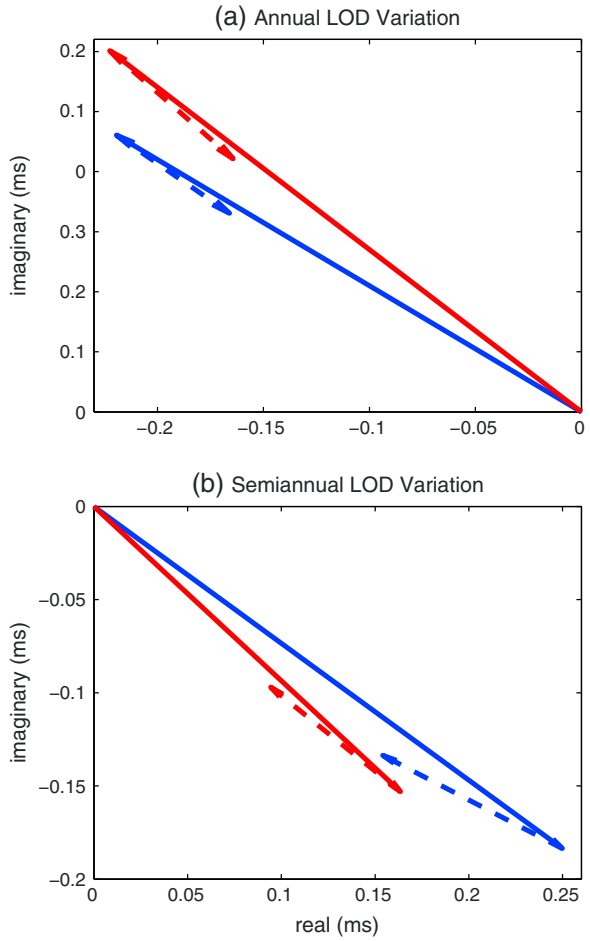

Figure 8. Phasor diagrams of the annual and semiannual LOD variations due to the atmospheric/cryospheric excitations (solid/dashed phasors) for the MY24/DS scenarios (blue/red phasors).

component. The excessively large cryospheric contribution to the *y* component of semiannual polar motion needs further investigations. In all, the GDS increases the amplitude of semiannual polar motion by 22%.

4.1.2. LOD Variations

[30] Figure 7 displays the axial excitation functions (χ_3) during months 1–12 in a Martian year for the MY24/DS scenarios (blue/red curves and open/closed circles). The curves are vertically shifted for clarity of display. The GDS influences are also discernible. The cryospheric excitation exhibits smaller variation than the atmospheric excitation. And it acts to weaken the atmospheric effect in general, as suggested by *Van den Acker et al*. [2002].

[31] The LOD variation is easily obtained from the meteorological excitation functions according to equation (2). Table 3 assembles the least-squares fitted amplitude and phase of the seasonal LOD variations for the MY24/DS scenarios. The amplitude of annual LOD variation from total atmospheric and cryospheric contributions for the MY24 scenario (0.234 ms) agrees well with *Defraigne et al*. [2000] (0.223 ms), *Van den Acker et al*. [2002] (0.253 ms), and *Karatekin et al*. [2011b] (0.229 ms) using current or previous MCD but differs to some extent from *Sanchez et al*. [2003] (0.374 ms) and *Karatekin et al*. [2011b] (0.360 ms) using the NASA Ames GCM. The MCD conforms slightly better to the observations than the NASA Ames GCM [*Konopliv et al*., 2011].

[32] The phasor diagrams of the annual and semiannual LOD variations due to the atmospheric/cryospheric excitations (solid/dashed phasors) for the MY24/DS scenarios (blue/red phasors) are shown in Figure 8. For the GDS signal, the atmospheric and cryospheric contributions increase the amplitude of annual LOD variation but decrease that of semiannual LOD variation. In sum, the GDS brings 15% increase in the amplitude of the annual LOD variation and 34% decrease in the amplitude of the semiannual LOD variation, some 10~20% larger than earlier results obtained by *Van den Acker et al*. [2002]. These quantitative differences presumably relate to the different versions of MCD data: the current MCD v4.3 covers longer spans than the previous MCD v3.0, which provides a more comprehensive view of the GDS effect.

[33] Figure 9 illustrates the seasonal LOD variations (unit in ms) determined from the MCD MY24/DS scenarios (black/red curves) and from the space observations of *Konopliv et al*. [2006] (green region) and *Konopliv et al*. [2011] (blue region). The modeled LOD during each of months 1–12 is fitted by spline to the set of values at corresponding Martian solar longitudes, with resolution 1°, from 0 to 360°. The thickness of the shadowed regions represents the measurement uncertainties. The additional Mars observational data of recent years improved the seasonal LOD determination by lowering the uncertainty of about 30% [*Konopliv et al*., 2011]. The MY24/DS seasonal LOD variations both appear to fall within the measurement uncertainty. Unfortunately, the modeled GDS signal is thus still buried in the observational noise.

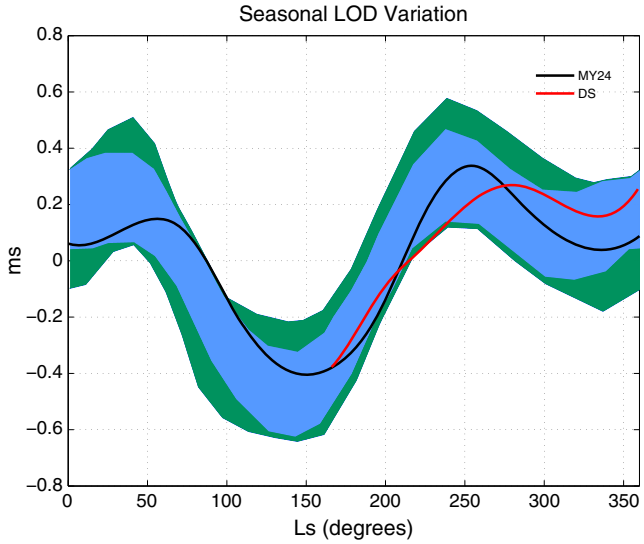

Figure 9. Seasonal LOD variations (unit in ms) for the MY24/DS scenarios (black/red curves). The observations from *Konopliv et al*. [2006] (green region) and *Konopliv et al*. [2011] (blue region) are shown for comparisons. The thickness of the shadowed regions represents the measurement uncertainties.

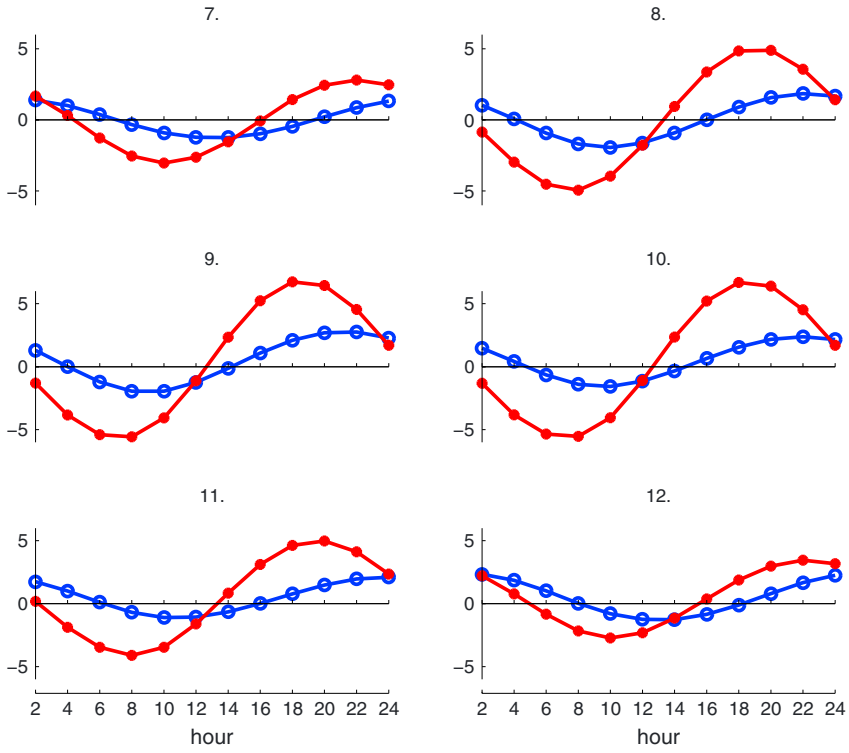

Figure 10. Daily variation pattern of the equatorial atmospheric excitation functions (χ_1^{atm}) during months 7–12 in the late half of a Martian year for the MY24/DS scenarios (blue/red curves and open/closed circles). Unit is 10^{-7}. The mean is removed from each series.

4.2. Diurnal and Semidiurnal Time Scales

[34] In this section, we have the opportunity for the first time to examine the highest frequencies of the excitation of Mars rotation, on the diurnal and semidiurnal time scales. This result is important in understanding the rapid fluctuations in Mars rotation, which relate to the tides and to reference frame issues on these time scales.

4.2.1. Polar Motion

[35] The GDS signal in the meteorological excitation of Mars' diurnal/semidiurnal rotation is investigated by comparing the daily variation patterns of Mars' rotational excitation functions for the MY24 and DS scenarios. Figure 10 shows the daily variation patterns of the equatorial atmospheric excitation functions (χ_1^{atm}) during months 7–12 in the late half of a Martian year for the MY24/DS scenarios (blue/red curves and open/closed circles). The χ_2^{atm} component (not shown) changes in a similar pattern as χ_1^{atm}. Evidently, the diurnal cycles of the equatorial atmospheric excitations increase significantly from the MY24 to the DS scenario, because of the stronger GDS-related atmospheric tide signal [e.g., *Bridger and Murphy*, 1998]. The atmospheric excitations for the DS scenario during the late half of a Martian year also reflect vividly the process of evolution of a great dust storm. In this case, it emerged in month 7 and reached to a severe stage in months 9 and 10 with a relaxation in month 12. The temporal evolution of the influence of the dust storm is clear here, unlike in earlier studies.

[36] The daily variations of equatorial cryospheric excitation functions for the MY24/DS scenarios (not shown)

Table 4. Amplitude and Phase of the Diurnal Polar Motion During Months 1–12 in a Martian Year for the MY24/DS Scenarios[a]

	MY24 Scenario		DS Scenario	
Month	Amplitude (mas)	Phase (deg)	Amplitude (mas)	Phase (deg)
	Polar motion: x component			
1	0.3	−136.4		
2	0.4	−152.2		
3	0.4	−158.9		
4	0.4	−157.4		
5	0.4	−152.9		
6	0.3	−135.1		
7	0.3	−109.3	0.6	−63.1
8	0.4	−61.3	1.0	−19.5
9	0.5	−46.9	1.2	−13.3
10	0.4	−56.4	1.2	−13.2
11	0.3	−77.6	0.9	−26.2
12	0.4	−107.3	0.6	−63.5
	Polar motion: y component			
1	0.4	−53.5		
2	0.4	−70.3		
3	0.4	−77.9		
4	0.4	−75.5		
5	0.4	−68.2		
6	0.3	−53.5		
7	0.3	−27.1	0.5	22.3
8	0.3	21.4	0.9	71.9
9	0.4	38.8	1.1	79.3
10	0.3	26.6	1.1	79.5
11	0.3	2.9	0.8	64.4
12	0.4	−27.0	0.5	20.4

[a]The phase angle refers to the beginning of a Martian day with respect to the sine convention.

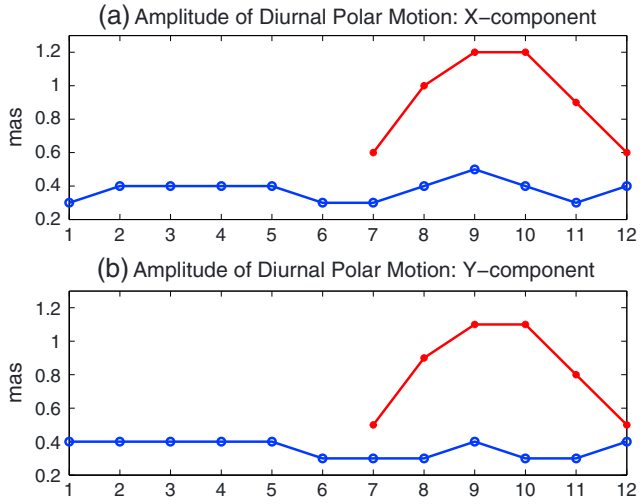

Figure 11. Amplitude of the diurnal polar motion for the MY24/DS scenarios (blue/red curves and open/closed circles) during months 1–12 in a Martian year.

Table 5. Amplitude and Phase of the Semidiurnal LOD Variation During Months 1–12 in a Martian Year for the MY24/DS Scenarios[a]

	MY24 Scenario		DS Scenario	
Month	Amplitude (ms)	Phase (deg)	Amplitude (ms)	Phase (deg)
1	0.003	−64.5		
2	0.003	−80.3		
3	0.002	−98.9		
4	0.003	−92.8		
5	0.003	−73.5		
6	0.003	−67.1		
7	0.003	−80.0	0.022	−63.0
8	0.006	−69.2	0.027	−58.5
9	0.007	−62.7	0.030	−54.0
10	0.006	−65.0	0.031	−53.7
11	0.005	−64.1	0.021	−56.7
12	0.004	−65.5	0.018	−61.3

[a]The phase angle refers to the beginning of a Martian day with respect to the sine convention.

are about 2 orders of magnitude smaller than the corresponding atmospheric excitations. While the cryospheric excitation plays a non-negligible role in the seasonal polar motion, its variability at these short time scales is completely negligible.

[37] The polar motion is computed from the meteorological excitation functions according to equation (1). Table 4 lists the least-squares fitted amplitude and phase of the diurnal polar motion (x and y component) during months 1–2 in a Martian year for the MY24/DS scenarios. The phase angle refers to the beginning of a Martian day with respect to the sine convention. Figure 11 displays the amplitude of the diurnal polar motion for the MY24/DS scenarios (blue/red curves and open/closed circles). As can be seen, the amplitude of diurnal polar motion during months 9 and 10 reaches about 3 times as large as that during the same stage in a typical Martian year.

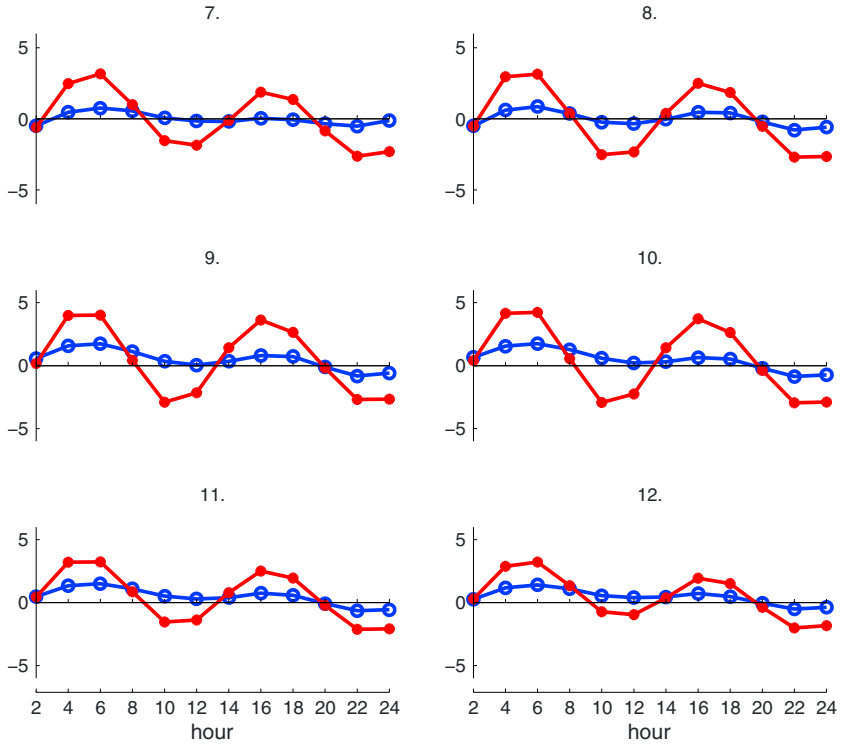

Figure 12. Daily variation pattern of the axial atmospheric excitation function (χ_3^{atm}) during months 7–12 in the late half of a Martian year for the MY24/DS scenarios (blue/red curves and open/closed circles). Unit is 10^{-10}. The mean is removed from each series.

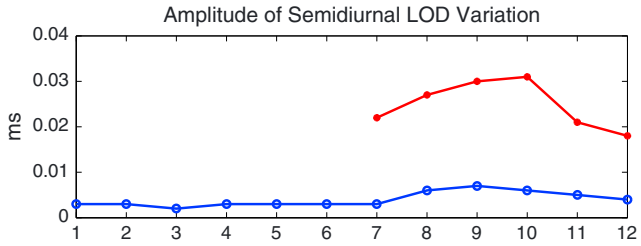

Figure 13. Amplitude of the semidiurnal LOD variation for the MY24/DS scenarios (blue/red curves and open/closed circles) during months 1–12 in a Martian year.

4.2.2. LOD Variations

[38] Figure 12 exhibits the daily variation patterns of the axial atmospheric excitation function (χ_3^{atm}) for the MY24/DS scenarios (blue/red curves and open/closed circles) during months 7–12 in the late half of a Martian year. Clearly, the DS scenario drastically enhances the semidiurnal cycles from the MY24 state, due to stronger atmospheric tides observed during the GDS period.

[39] The daily variations of axial cryospheric excitation functions for the MY24/DS scenarios (not shown) are about 1 order of magnitude smaller than the corresponding atmospheric excitations. As was the case above, the cryosphere does not have significant variability on subdiurnal scales.

[40] Table 5 assembles the least-squares fitted amplitude and phase of the semidiurnal LOD variation during months 1–12 in a Martian year for the MY24/DS scenarios. Figure 13 shows the amplitude of the semidiurnal LOD variation for the MY24/DS scenarios. The amplitude of semidiurnal LOD variation during month 10 goes up to about 5 times as large as that during the same stage in a typical Martian year.

5. Summary and Discussion

[41] At first, the GDS signal in the meteorological excitation of Mars' rotation is investigated comprehensively on seasonal time scales, using the updated MCD v4.3 data set. Due to its location at high latitudes, where the weighting function on polar motion and LOD excitations is low, the cryospheric excitation plays in general a less important role than its atmospheric counterpart, though it is still non-negligible. The GDS brings (−3%, +15%) changes in the amplitude of annual polar motion and LOD variation and (+22%, −34%) changes in the amplitude of semiannual polar motion and LOD variation.

[42] For the first time, we have been able to explore the short periodic diurnal/semidiurnal GDS signal in the meteorological excitation of Mars' rotation. For this time scale, the cryospheric excitation can be neglected in comparison to its atmospheric counterpart. Significant GDS signals are found owing to strong atmospheric tides in the GDS period. The amplitude increases in diurnal polar motion and semidiurnal LOD variation in some months may reach 3–5 times as large as those during the same stage in a typical Martian year.

[43] The atmospheric tides are large-scale periodic oscillations of the atmosphere excited gravitationally or thermally [*Chapman and Lindzen*, 1970]. The presence of thermally driven tides in the Martian atmosphere, forced by the solar heating, has been firmly established from space observations and numerical simulations [*Bridger and Murphy*, 1998]. The thermal tides, at diurnal and semidiurnal periods, are enhanced significantly during GDS periods, due to the strong absorption of solar radiation by suspended dusts [*Leovy and Zurek*, 1979; *Murphy et al*., 1995; *Lewis and Barker*, 2005]. They cause a large amount of angular momentum transfer between the global atmosphere and the solid planet below [*Munk and MacDonald*, 1960; *Wilson and Hamilton*, 1996; *Heavens et al*., 2011], thereby leading to significant short periodic variations in Mars' rotation.

[44] It is worth noting however that the estimates of GDS effects are susceptible to modeling errors. Mass and zonal winds from the NASA Ames GCM are some 30% larger than the MCD [*Konopliv et al*., 2011], and the related annual and semiannual LOD variations computed from these models yield about 20–40% differences [*Karatekin et al*., 2011b]. Hopefully, such modeling uncertainties will be reduced in future assimilations using new accurate space observations of Mars [*Millour et al*., 2011].

[45] A number of scientific missions are planned to explore Mars. For instance, the NASA 2016 InSight (Interior Exploration using Seismic Investigations, Geodesy and Heat Transport) Lander mission will use the spacecraft communication and navigation system to provide precise measurements of Mars' rotation (http://insight.jpl.nasa.gov/mission/). The ESA ExoMars 2016 mission will include the Trace Gas Orbiter and the ExoMars Entry, Descent and Landing Demonstrator Module (EDM) to study the GDS impact on the general circulation [*Forget et al*., 2011].

[46] As the determination of Mars' rotational parameters improves with more accurate tracking of Mars orbiters and landers [*Rosenblatt and Dehant*, 2010; *Konopliv et al*., 2011], the GDS effect on Mars' rotation could be detected in the future if the measurement accuracy of Mars' rotation becomes as high as that of current space-geodetic monitoring of the Earth (e.g., sub-milliarcsecond for polar motion and microsecond for the LOD change). Comparisons between observations and model-based rotational results at the highest frequencies, such as subdiurnal, should deepen our understanding of the nature of Mars' rotation and the influence of the atmosphere. Furthermore, the highly accurate observation of the GDS effect on Mars' rotation should also provide an independent way to constrain, validate, and improve Mars general circulation models.

[47] **Acknowledgments.** We are grateful to M. Wieczorek, Ö. Karatekin, B.V. Sanchez, and two anonymous reviewers for their insightful comments and encouragements, which led to improvements in the presentation. We thank F. Forget for providing us the Mars Climate database and X. Y. Zhuo for plotting the figures. Y.H.Z., X.Q.X., and X.H.L. were supported by the NSFC grant (11073045, 11133004), CAS (KJCX2-YW-T13), and STCSM (06DZ22101). D.S. was supported by the US National Science Foundation under grant ATM-0913780.

References

Barnes, R., R. Hide, A. White, and C. R. Wilson (1983), Atmospheric angular momentum fluctuations, length-of-day changes and polar motion, *Proc. R. Soc. Lond.*, *387*, 31–73.

Bridger, A. F. C., and J. R. Murphy (1998), Mars' surface pressure tides and their behavior during global dust storms, *J. Geophys. Res.*, *103*(E4), 8,587–8,601.

Cantor, B. A. (2007), MOC observations of the 2001 Mars planet-encircling dust storm, *Icarus*, *186*, 60–96, doi:10.1016/j.icarus.2006.08.019.

Cazenave, A., and G. Balmino (1981), Meteorological effects on the seasonal variations of the rotation of Mars, *Geophys. Res. Lett.*, *8*(3), 245–248.

Chao, B. F., and D. P. Rubincam (1990), Variations of Mars gravitational field and rotation due to seasonal CO_2 exchange, *J. Geophys. Res.*, *95*(B9), 14,755–14,760.

Chapman, S., and R. S. Lindzen (1970), *Atmospheric Tides*, D. Reidel Publishing Company, Dordrecht, Holland.

Clancy, R. T., B. J. Sandor, M. J. Wolff, et al. (2000), An intercomparison of ground-based millimeter, MGS TES, and Viking atmospheric temperature measurements: Seasonal and interannual variability of temperatures and dust loading in the global Mars atmosphere, *J. Geophys. Res.*, *105*(E4), 9553–9571, doi:10.1029/1999JE001089.

Defraigne, P., O. de Viron, V. Dehant, T. Van Hoolst, and F. Hourdin (2000), Mars rotation variations induced by atmosphere and ice caps, *J. Geophys. Res.*, *105*(E10), 24,563–24,570.

Elteto, A., and B. T. Owen (2010), The effects and characteristics of atmospheric dust during martian global dust storm 2001A, *Icarus*, *210*, 589–611, doi:10.1016/j.icarus.2010.07.011.

Eubanks, T. M. (1993), Variations in the orientation of the Earth, in *Contributions of Space Geodesy to Geodynamic: Earth Dynamics*, Geodyn. Ser., edited by D. Smith, and D. Turcotte, pp. 1–54, AGU, Washington, D.C.

Folkner, W. M., C. F. Yoder, D. N. Yuan, E. M. Standish, and R. A. Preston (1997), Interior structure and seasonal mass redistribution of Mars from radio tracking of Mars Pathfinder, *Science*, *278*, 1749–1751.

Forget, F., F. Hourdin, R. Fournier, C. Hourdin, O. Talagrand, M. Collins, S. R. Lewis, P. L. Read, and J.-P. Huot (1999), Improved general circulation models of the Martian atmosphere from the surface to above 80 km, *J. Geophys. Res.*, *104*(E10), 24,155–24,176.

Forget, F., A. Spiga, L. Montabone, E. Millour, A. Colaitis, V. Bourrier, and S. Portigliotti (2011), Characterizing the Martian atmosphere for the ExoMars 2016 lander, paper presented at the Fourth International Workshop on the Mars Atmosphere: Modelling and Observation, CNES, 8–11 February.

Gawrych, J. M. (2007), The 2001 Martian global dust storm, Ph.D. thesis, 107 pp., San Jose State Univ., San Jose, Calif.

Haberle, R. M., M. M. Joshi, J. R. Murphy, J. R. Barnes, J. T. Schofield, G. Wilson, M. Lopez-Valverde, J. L. Hollingsworth, A. F. C. Bridger, and J. Schaeffer (1999), General circulation model simulations of the Mars Pathfinder atmospheric structure investigation/meteorology data, *J. Geophys. Res.*, *104*(E4), 8957–8974.

Heavens, N. G., D. J. McCleese, M. I. Richardson, et al. (2011), Structure and dynamics of the Martian lower and middle atmosphere as observed by the Mars Climate Sounder: 2. Implications of the thermal structure and aerosol distributions for the mean meridional circulation, *J. Geophys. Res.*, *116*, E01010, doi:10.1029/2010JE003713.

Hourdin, F., P. Le Van, F. Forget, and O. Talagrand (1993), Meteorological variability and the annual surface pressure cycle on Mars, *J. Atmos. Sci.*, *50*, 3625–3640.

Hourdin, F., F. Forget, and O. Talagrand (1995), The sensitivity of the Martian surface pressure to various parameters: A comparison between numerical simulations and Viking observations, *J. Geophys. Res.*, *100*, 5501–5523.

Karatekin, Ö., T. VanHoolst, J. Tastet, O. de Viron, and V. Dehant (2006a), The effects of seasonal mass redistribution and interior structure on length-of-day variations of Mars, *Adv. Space Res.*, *38*(4), 739–744, doi:10.0002/JASR-D-04-01301R1.

Karatekin, Ö., T. Van Hoolst, and V. Dehant (2006b), Martian global-scale CO_2 exchange from time-variable gravity measurements, *J. Geophys. Res.*, *111*, E06003, doi:10.1029/2005JE002591.

Karatekin, Ö., O. de Viron, S. Lambert, V. Dehant, P. Rosenblatt, T. Van Hoolst, and S. Le Maistre (2011a), Atmospheric angular momentum variations of Earth, Mars and Venus at seasonal time scales, *Planet. Space Sci.*, *59*, 923–933.

Karatekin, Ö., A. S. Konopliv, and C. Yoder (2011b), Martian CO_2 cycle from time-variable gravity and LOD observation, paper presented at the Fourth International Workshop on the Mars Atmosphere: Modelling and Observation, CNES, 8–11 February.

Konopliv, A. S., C. F. Yoder, E. M. Standish, D. N. Yuan, and W. L. Sjogren (2006), A global solution for the Mars static and seasonal gravity, Mars orientation, Phobos and Deimos masses, and Mars ephemeris, *Icarus*, *182*, 23–50.

Konopliv, A. S., S. W. Asmar, W. M. Folkner, Ö. Karatekin, D. C. Nunes, S. E. Smrekar, C. F. Yoder, and M. T. Zuber (2011), Mars high resolution gravity fields from MRO, Mars seasonal gravity, and other dynamical parameters, *Icarus*, *211*, 401–428.

Lambeck, K. (1980), *The Earth's Variable Rotation: Geophysical Causes and Consequences*, Cambridge Univ. Press, New York.

Leovy, C. B., and R. W. Zurek (1979), Thermal tides and Martian dust storms: Direct evidence for coupling, *J. Geophys. Res.*, *84*(B6), 2956–2968, doi:10.1029/JB084iB06p02956.

Lewis, S. R., and P. R. Barker (2005), Atmospheric tides in a Mars general circulation model with data assimilation, *Adv. Space Res.*, *36*(11), 2162–2168.

Lewis, S. R., M. Collins, P. L. Read, F. Forget, et al. (1999), A climate database for Mars, *J. Geophys. Res.*, *104*(E10), 24,177–24,194.

Litvak, M. L., I. G. Mitrofanov, A. S. Kozyrev, et al. (2004), Seasonal carbon dioxide depositions on the Martian surface as revealed from neutron measurements by the HEND instrument onboard the 2001 Mars Odyssey spacecraft, *Solar Sys. Res.*, *38*(3), 167–177.

Millour, E., et al. (2011), An improved Mars climate database, paper presented at the Fourth International Workshop on the Mars Atmosphere: Modelling and Observation, CNES, 8–11 February.

Munk, W. H., and G. J. F. MacDonald (1960), *The Rotation of the Earth: A Geophysical Discussion*, Cambridge Univ. Press, New York.

Murphy, J. R., J. B. Pollack, R. M. Haberle, C. B. Leovy, O. B. Toon, and J. Schaeffer (1995), Three-dimensional numerical simulation of Martian global dust storms, *J. Geophys. Res.*, *100*(E12), 26,357–26,376, doi:10.1029/95JE02984.

Philip, J. R. (1979), Angular momentum of seasonally condensing atmospheres, with special reference to Mars, *Geophys. Res. Lett.*, *6*(9), 727–730.

Rosenblatt, P., and V. Dehant (2010), Mars geodesy, rotation and gravity, *Res. Astron. Astrophys.*, *10*, 713, doi:10.1088/1674-4527/10/8/002.

Sanchez, B. V., D. D. Rowlands, R. M. Haberle, and J. Schaeffer (2003), Atmospheric rotational effects on Mars based on the NASA Ames general circulation model, *J. Geophys. Res.*, *108*(E5), 5040, doi:10.1029/2002JE001984.

Sanchez, B., R. Haberle, and J. Schaeffer (2004), Atmospheric rotational effects on Mars based on the NASA Ames general circulation model: Angular momentum approach, *J. Geophys. Res.*, *109*, E08005, doi:10.1029/2004JE002254.

Smith, M. D. (2008), Spacecraft observations of the Martian atmosphere, *Annu. Rev. Earth Planet. Sci.*, *36*, 191–219, doi:10.1146/annurev.earth.36.031207.124334.

Smith, D. E., M. T. Zuber, R. M. Haberle, D. D. Rowlands, and J. R. Murphy (1999), The Mars seasonal CO_2 cycle and the time variation of the gravity field: A general circulation model simulation, *J. Geophys. Res.*, *104*(E1), 1885–1896.

Smith, D. E., M. T. Zuber, and M. Neumann (2001), Seasonal variations of snow depth on Mars, *Science*, *294*, 2141–2146.

Van den Acker, E., T. Van Hoolst, O. de Viron, P. Defraigne, F. Forget, F. Hourdin, and V. Dehant (2002), Influence of the seasonal winds and the CO_2 mass exchange between atmosphere and polar caps on Mars' rotation, *J. Geophys. Res.*, *107*(E7), 5055, doi:10.1029/2000JE001539.

Van Hoolst, T., V. Dehant, and P. Defraigne (2000), Chandler wobble and free core nutation for Mars, *Planet. Space Sci.*, *48*, 1145–1151.

Wieczorek, M. A. (2007), Gravity and topography of the terrestrial planets, *Treatise on Geophys.*, *10*, 165–205, doi:10.1016/B978-044452748-6/00156-5.

Wilson, R. J., and K. Hamilton (1996), Comprehensive model simulation of thermal tides in the Martian atmosphere, *J. Atmos. Sci.*, *53*, 1290–1326.

Yoder, C. F., and E. M. Standish (1997), Martian precession and rotation from Viking lander range data, *J. Geophys. Res.*, *102*(E2), 4065–4080.

Yoder, C. F., A. S. Konopliv, D. N. Yuan, E. M. Standish, and W. M. Folkner (2003), Fluid core size of Mars from detection of the solar tide, *Science*, *300*, 299–303.

Zhou, Y. H., D. A. Salstein, J. L. Chen (2006), Revised atmospheric excitation function series related to Earth's variable rotation under consideration of surface topography, *J. Geophys. Res.*, *111*, D12108, doi:10.1029/2005JD006608.

Zurek, R. W., and L. J. Martin (1993), Interannual variability of planet-encircling dust storms on Mars, *J. Geophys. Res.*, *98*, 3247–3259.